Photoresponse Model for $Si_{1-x}Ge_x/Si$ Heterojunction Internal Photoemission Long-wavelength Infrared Detector

T. L, Lin, J. S. Park, S. D. Gunapala, E. W. Jones, and H. M. Del Castillo
Center for Space Microelectronics Technology
Jet Propulsion Laboratory, California Institute of Technology
Pasadena, CA 91109

ABSTRACT

A photoresponse model has been developed for the $Si_{1-x}Ge_x/Si$ heterojunction internal photoemission (311P) infrared detector at wavelengths corresponding to photon energies less than the Fermi energy. A $Si_{0.7}Ge_{0.3}/Si$ HIP detector with a cutoff wavelength of 23 pm and an emission coefficient of 0.4 eV^{-1} has been demonstrated. The model agrees with the measured detector response at $\lambda > 8$ μm. The potential barrier determined by the model is in close agreement (difference -4 meV) with the potential barrier determined by the Richardson plot, compared to the discrepancies of 20-50 meV usually observed for PtSi Schottky detectors.

I. INTRODUCTION

Previously, SixGel -x/Si heterojunction internal photoemission (HIP) long-wavelength infrared (LWIR) detectors [1-51, and 400 x 400-element imager arrays have been demonstrated [4,5]. The concept of utilizing free-carrier absorption and internal photoemission over a heterojunction barrier for JR detection was first proposed by Shepherd *et. al.* [6]. The advantage of the Si_xGe_{1-x}/Si HIP detectors is that they are fabricated on Si substrates, and consequently can be integrated with Si readout multiplexers to form large LWIR focal plane arrays. The Si_xGe_{1-x}/Si HIP detector is essentially a p^+-Si_xGe_{1-x}/p-Si heterojunction unipolar diode, which responds to infrared radiation via free-carrier absorption in the degenerately doped $Si_{1-x}Ge_x$ layer followed by the internal photoemission of photo-excited holes over the Si_xGe_{1-x}/Si heterojunction barrier into the Si substrate. The cutoff wavelength of the Si_xGe_{1-x}/Si HIP detector, determined by the optical potential barrier 'l'., is given by

$$\lambda_c = \frac{1.24}{\Psi_o} = \frac{1.24}{\Delta E_v - (E_F - E_v)} \qquad (1)$$

where ΔE_v is the Si_xGe_{1-x}/Si valence band offset. This offset increases with increasing Ge composition in the Si_xGe_{1-x} layer. E_v and E_F are the. valence band energy ant] the Fermi energy of the Si_xGe_{1-x} layer, respectively. The cutoff wm~e.length of the Si_xGe_{1-x}/Si HIP detector can be tailored to the LWIR region by reducing the Ge composition and increasing the boron doping concentration of the Si_xGe_{1-x} layer[1,2,5]. Furthermore, due to the increasing free-carrier absorption with increasing wavelength and dopant concentration [2,3], the Si_xGe_{1-x}/Si HIP detector is well-suited for 1.WIR detection, in which degenerate boron doping concentrations are desirable for efficient detector operation.

The spectral response of the $Si_{1-x}Ge_x/Si$ 1111' detector differs from that of other internal photoemission detectors, such as the PtSi Schottky detector. For the silicide Schottky detector, the spectral response is given by the modified Fowler equation [7]:

$$\eta = C_1 \frac{(h\nu - \Psi_0)^2}{h\nu} = 1.24\, C_1 \lambda \left(\frac{1}{\lambda} - \frac{1}{\lambda_c}\right)^2 \qquad (2)$$

where Cl is the Fowler emission coefficient, hv is the photon energy, Ψ_0 is the optical potential barrier, λ is the wavelength, and λ_c is the cutoff wavelength, given by $\lambda_c = 1.24/\Psi_0$. The Fowler emission coefficient C_1 is given by

$$C_1 = \frac{A}{8 E_F} \qquad (3)$$

where A is the absorptance and E_F is the Fermi energy. The optical potential barrier Y'. can be determined from the detector spectral response by linearizing Eq. (2):

$$\sqrt{\eta\, h\nu} = \sqrt{C_1}\,(h\nu - \Psi_0) \qquad (4)$$

in contrast to the spectral response of the silicide Schottky detector, which decreases monotonically with increasing wavelength (Eq. 2), the response of the Si_xGe_{1-x}/Si HIP detector increases initially with increasing wavelength, and then decreases monotonically to zero at the cutoff wavelength [1-5]. Consequently, the modified Fowler equation is not applicable to the Si_xGe_{1-x}/Si HIP detector. This is due to two major differences between the semiconductor properties of the degenerately doped p-t ypc $Si_{1-x}Ge_x$ layer and the metallic properties of the silicide. First, the IR absorption of the $Si_{1-x}Ge_x$ layer increases with increasing wavelength, as compared to the wavelength-independent absorption for the sil icide. Second, t he Fermi energ y of the $Si_{1-x}Ge_x$ layer is significantly smaller than that of the silicide. For the silicide, the Fermi energy is much larger than the photon energy and the density of states is approximately energy-independent in an energy range from E_F to (E_F -t- hv). For the $Si_{1-x}Ge_x$, the Fermi energy is determined by the doping concentration, and the density of states g(E) is given by

$$g(E) = N\,(E - E_V)^{0.5}, \qquad (5)$$

where N is an energy-independent constant,

Previously, a theoretical model for the internal quantum efficiency of the Si_xGe_{1-x}/Si HIP detector was reported by Tsaur *et al.* [5]. The model was developed for the region $h\nu >> E_F$, and the wavelength-dependent absorption was not considered. Because degenerate boron concentrations in the Si_xGe_{1-x} layers are usually required to obtain a strong infrared absorption, the Fermi energies are usually several hundred meV. For example, an estimated Fermi energy of 0.15 eV has been previously reported [2,3]. Therefore, the previous model can only be applied in the shorter wavelength regime, i.e., for $\lambda << 1.24/E_F$, and is not applicable for the determination of the optical potential barrier Ψ_0.

The determination of the optical potential barrier Ψ_0 of the Si_xGe_{1-x}/Si HIP detector is critical for the study of the potential discrepancy between the optical and the thermal potential barriers. Previously, it has been reported that for the silicide Schottky detector, the thermal barrier Ψ_t is usually 20-50 meV lower than the optical barrier Ψ_0 [6]. As a result, more cooling is required for the silicide Schottky detector compared to detectors with the same cutoff wavelength but without the discrepancy in potential. The cooling penalty worsens as the cutoff wavelength increases and the potential discrepancy becomes comparable to the decreasing

potential barrier. The thermal potential barrier Ψ_t of the Si_xGe_{1-x}/Si HIP detector can be determined by the Richardson's plot:

$$\ln\left(\frac{J_0}{T^2}\right) = -\frac{\Psi_t}{kT} + \text{in (A**)}. \qquad (6)$$

The dark current density Jo is dominated by the thermionic emission current [3-5], given by the Richardson equation:

$$J_o = A^{**} T^2 \exp(-\Psi_t / kT), \qquad (7)$$

where A** is the Richardson constant, 'J" is the absolute temperature, and k is Boltzmann constant. Therefore, a response model for the determination of the optical potential barrier of the Si_xGe_{1-x}/Si HIP detector is required for the study of the potential barrier discrepancy.

Furthermore, it is important to model the detector response c1osc to the cutoff wavelength, since a fast response increase as the wavelength decreases from the cutoff will allow the detector to have useful sensitivity near the cutoff, thereby minimizing the extension of the cutoff wavelength and associated cooling requirements. Thus, a response model which predicts the detector response at wavelengths near the cutoff wavelength will not only determine. the optical potential barrier Ψ_o, but also provide a figure-of-merit for evaluating the Si_xGe_{1-x}/Si HIP detector.

In this paper, a response model for the Si_xGe_{1-x}/Si HIP detector is presented. The model predicts the spectral response at wavelengths ranging from the wavelength corresponding to the Fermi energy to the cutoff wavelength. A $Si_{0.7}Ge_{0.3}/Si$ HIP detector with a 23 μm cutoff wavelength has been fabricated and characterized. The detector photoresponse agrees with the prediction of the theoretical model. The optical barrier of the $Si_{0.7}Ge_{0.3}/Si$ HIP detector has been determined by the model and compared with the thermal barrier.

II. THEORETICAL MODEL

The quantum efficiency (QE) is defined as the ratio of the collected holes N_c to the incident photons Np, *i.* e.,

$$\eta = \frac{N_c}{N_p} = A\,\frac{N_c}{N_T} \qquad (8)$$

where NT is the number of photo-excited holes. Under the zero-temperature approximation, and assuming $E_V = O$, N_c is given by

$$N_c = \int_{E_F+\Psi_O}^{E_F+h\nu} g(E)\,p(E)\,dE = \int_{E_F+\Psi_O}^{E_F+h\nu} NE^{0.5}\,\frac{1}{2}\left(1-\sqrt{\frac{E_F+\Psi_O}{E}}\right)dE$$

$$\cong \frac{\pi}{8} N \frac{(h\nu-\Psi_O)^2}{(E_F+\Psi_O)^{1/2}} \qquad \text{for } h\nu \geq \Psi_O. \qquad (9)$$

where g(E) is the density of states given by Eq. 5 and p(E) is the probability of emission of photo-excited holes over the energy barrier, given by

$$p(E) = \frac{1}{2}\sqrt{\left(1-\frac{E_F+\Psi_0}{E}\right)} \qquad (10)$$

because a momentum normal to the $Si_{1-x}Ge_x/Si$ interface with a corresponding energy greater than $E_F+\Psi_0$ is required for the emission of photo-excited holes.

As mentioned previously, determining the optical barrier and the spectral response near the cutoff wavelength are the primary concerns, so the analysis will be limited to the case $h\nu < E_F$. Due to the degenerate doping concentration of the $Si_{1-x}Ge_x$ layer, holes populate states from the edge of the valence band to the Fermi level. The number of photo-excited holes, N_T, is given by

$$N_T = \int_{E_F}^{E_F+h\nu} NE^{0.5}\,dE$$

$$\cong N\,h\nu\,E_F^{0.5} \qquad \text{for } h\nu << E_F. \qquad (11)$$

Therefore, η is given by

$$\eta = \frac{A}{813F0.5\,(E_F+\Psi_0)^{0.5}}\,\frac{(h\nu-\Psi_0)^2}{h\nu}$$

$$= C_h\frac{(h\nu-\Psi_0)^2}{h\nu} \qquad (12)$$

where the emission coefficient C_h is given by

$$C_h = \frac{A}{8\,E_F^{0.5}\,(E_F+\Psi_0)^{0.5}}, \qquad (13)$$

because the infrared absorptance A is relatively wavelength-independent in the long wavelength region as reported previously [2,3]. Thus, the photoresponse of the Si_xGe_{1-x}/Si HIP detector for $h\nu << E_F$ can be modeled by Eq. 12, which is similar to the modified Fowler equation. Both the optical potential barrier Ψ_0 and the emission coefficient C_h for the Si_xGe_{1-x}/Si HIP detector can be determined by the plot of $\sqrt{\eta h\nu}$ versus $h\nu$ for $h\nu << E_F$. The similarity between this model and the modified Fowler equation is due to the fact that photons with energy $h\nu << E_F$ can only excite holes populating states from E_F-$h\nu$ to E_F in the degenerate] y doped $Si_{0.7}Ge_{0.3}$ layer, which is similar to the case for the Schottky detector.

111. DETECTOR FABRICATION

The $Si_{0.7}Ge_{0.3}/Si$ HIP detector was fabricated by growing hetero-epitaxial $Si_{0.7}Ge_{0.3}$ layers on double-side polished p-type Si (1O0)) wafers by molecular beam epitaxy (MBE) which provided abrupt and tailored doping profiles and a good crystal linity[3]. The device structure, incorporates pi--substrate contacts and n-type guard rings which define the periphery of the active device areas to suppress edge leakage. Prior to the MBE growth, the wafers were cleaned using the "spin-clean" method, which involves the removal of' a chemically grown surface oxide

using an HF/ethanol solution in a nitrogen glove box[9]. The p^+-$Si_{0.7}Ge_{0.3}$ layer was grown in a commercial Riber EVA 32 Si MBE system at a substrate temperature of 350 °C. Elemental boron was used as the dopant source during the MBE growth to achieve a doping concentration of 5 x 10^{20} cm^{-3}. The $Si_{0.7}Ge_{0.3}$ layer was 10 nm thick.

IV. DETECTOR CHARACTERISTICS

The reverse current-voltage (I-V) characteristics of the $Si_{0.7}Ge_{0.3}$/Si HIP detector were measured at temperatures ranging from 25 to 50 K. Figure 2 shows the reverse-bias I-V characteristics of a typical 10-rim-thick $Si_{0.7}Ge_{0.3}$/Si HIP detector with a detector area of 1.2 x 10-3 cm^2. The dark current of the $Si_{0.7}Ge_{0.3}$/Si HIP detector was dominated by the thermionic emission current. Figure 3 shows the plot of J_o/T^2 vs 1/kT of the $Si_{0.7}Ge_{0.3}$/Si 111P detector at -0.5 V bias. The active area of the detector was 1.2 x 10^{-3} cm^2. A thermal potential bat-rim- Ψ_t of 0.050 eV was determined from the slope of the linear portion. The effective barrier Ψ_t was significantly lower than the expected valence band offset ΔE_V (-0.2 eV) between Si and $Si_{0.7}Ge_{0.3}$ due to the degenerate doping concentration (5 x $10^{20}cm^{-3}$) of the $Si_{0.7}Ge_{0.3}$ layer which moves the Fermi level below the valence band edge, i.e.,

$$\Psi_t = \Delta E_V - E_F \qquad (14)$$

From Eq. (14), the Fermi energy E_F in the degenerately doped $Si_{0.7}Ge_{0.3}$ layer was estimated to be -0.15 eV. Therefore, for $\lambda > 8\,\mu m$, Eq. 12 can be used as a model for the photoresponse of the $Si_{0.7}Ge_{0.3}$/Si HIP detector.

The external quantum efficiency η for the $Si_{0.7}Ge_{0.3}$/Si HIP detector is shown in Fig. 4. The detector was cooled to 30K and biased at -0.5 V. The spectral response was measured with front-side illumination using a 940K blackbody source. Also shown in Fig. 4 is the spectral response of a doping-spike PtSi Schottky detector [10] with $C_1 = 0.15\ eV^{-1}$, $\Psi_t = 0.032$ eV, and Y'. = 0.056 eV, corresponding to a cutoff wavelength of 22.1 μm for comparison. Neither the $Si_{0.7}Ge_{0.3}$/Si HIP detector nor the doping-spike PtSi detector had an optical cavity or an anti-reflection coating. The doping-spike PtSi detector was cooled to 20 K and back-side illuminated. The QE of the doping-spike PtSi detector decreased with increasing wavelength, while the QE of $Si_{0.7}Ge_{0.3}$/Si HIP detector increased initially with increasing wavelength to -8 % at 4-5 μm, and then decreased because of the decreasing internal photoemission probability over the heterojunction barrier as the energy of the photo-excited carriers decreased. The initial increase of efficiency of the $Si_{0.7}Ge_{0.3}$/Si HIP detector resulted from the increase of the free-carrier. absorption 11]. At wavelengths larger than 2 μm, the QE of the $Si_{0.7}Ge_{0.3}$/Si HJP detector was significantly higher than that of the doping-spike PtSi detector.

Figure 5 shows the plot of $\sqrt{\eta}\,h\nu$ versus $h\nu$ for the $Si_{0.7}Ge_{0.3}$/Si HIP detector. As predicted by the preceding analysis, for $h\nu << E_F$ (Eq. 11) the plot was linear, and both C_h and Ψ_o can be determined from the slope and the intercept of the linear portion. An optical potential barrier Y'. of 0.054 eV, corresponding to a cutoff wavelength of 23 pm, was determined. in contrast to the 24 meV and the 20-50 meV potential discrepancies observed for the LWIR doping-spike PtSi detector [10] and the conventional PtSi detectors reported previous] y [6], a small difference between the optical barrier (0.054 eV) and the thermal potential barrier (0.0.50 cV) was observed for the $Si_{0.7}Ge_{0.3}$/Si HIP detector, suggesting that the photo-excited holes suffer less inelastic scattering in the $Si_{0.7}Ge_{0.3}$ layers. The coefficient C_h was determined to be ().4 eV^{-1} for the $Si_{0.7}Ge_{0.3}$/Si HIP detector, compared to a 0.15 eV^{-1} C1 for the doping-spike PtSi detector [7]. The larger emission coefficient of the $Si_{0.7}Ge_{0.3}$/Si HIP detector resulted

mainly from its smaller Fermi energy [10], The 0.4 eV^{-1} C_h observed was approximately twice the calculated value of 0.18 eV^{-1} from Eq. 13 because the model did not take the scattering of the photo-excited carriers into consideration. Elastic scattering of carriers at the Si_xGe_{1-x} surface redirected the carriers toward the Si_xGe_{1-x}/Si interface, and thus increased the emission coefficient.

V. SUMMARY

A model has been proposed for the spectral response of the Si_xGe_{1-x}/Si HIP detector at wavelengths with corresponding photon energies less than the Si_xGe_{1-x} Fermi energy. The model agrees with the spectral response of the $Si_{0.7}Ge_{0.3}/Si$ HIP detector at $\lambda > 8\,\mu m$. Similar optical and thermal barriers *were* observed for the $Si_{0.7}Ge_{0.3}/Si$ HIP detector, in contrast to the 20-50 meV discrepancies usually observed for PtSi Schottky infrared detectors. An emission coefficient C_h of 0.4 eV^{-1} was determined for the HIP detector with a 10-rim-thick $Si_{0.7}Ge_{0.3}$ layer doped with 5 x 10^{20} cm^{-3} boron.

ACKNOWLEDGMENTS

The work described in this report was performed by the Center for Space Microelectronics Technology, Jet Propulsion laboratory, California Institute of Technology and was jointly sponsored by the National Aeronautics and Space Administration/Office of Advanced Concepts and Technology, the Ballistic Missile Defense Organization/Innovative Science and "1'ethnology Office, and the Air Porte Rome laboratory.

REFERENCES

[1] T. L. Lin and J. Maserjian, "Novel p^+-$Si_{1-x}Ge_x$/p-Si heterojunction infrared detectors fabricated by molecular beam epitaxy," *Appl. Phys. Lett.*, vol. 57, pp. 1422-1424,1990.

[2] T. 1.. Lin, A. Ksendzov, S. M. Dejewski, E. W. Jones, R. W. Fathauer, T. N. Krabach and J. Maserjian, "SiGe/Si heterojunction internal photoemission long wavelength infrared detectors fabricated by molecular beam epitax y, " *IEEE Trans.* Electron *Devices, vol.* 38, 1141-1144, 1991.

[3] T. L. Lin, T. George. E. W. Jones A. Ksendzov and M. L. Huberman, "Elemental boron-doped p^+-SiGe layers grown by molecular beam epitaxy for infrared detector applications," *Appl. Phys. Lett.*, vol. 60, pp. 380-382, 1992

[4] B-Y. Tsaur, C. K. Chen and S. A. Marine, "1 .ong-wavelength Ge_xSi_{1-x}/Si heterojunction infrared detectors and 400 x 400-cl ement imager arrays," *IEEE Electron Device Lett.*, vol. 12, pp. 293-296, 1991.

[5] B-Y. Tsaur, C. K. Chen and S. A. Marine, "1 ,ong-wavelength Ge_xSi_{1-x}/Si heterojunction infrared detectors and focal plane arrays," *SPIE Proceedings*, vol. *1540,* pp. 580-595, 1991.

[6] F. D. Shepherd, Jr., V. E. Vickers, and A. C. Yang, "Schottky-barrier photodiode with a degenerate semiconductor active region," United States Patent 3,603,$47, September 7, 1971.

[7] V. 1.. Dalal, "Simple model for internal photoemission," J. Appl. Phys., vol. 42, pp. 2274-2279, 1971.

[8] F. D. Shepherd, "Infrared internal emission detectors, " *SPIE Proceedings*, Vol. 1735, *Infrared Detectors: State of the Art*, edited by W. H. Makky, pp. 250-261, 1992.

[9] P. J. Grunthaner, F. J. Grunthaner, R. W. Fathauer, '1'. L. Lin, M. H. Hecht, L. D. Bell, W. J. Kaiser, F. D. Schowengerdt, and J. H. Mazur, "Hydrogen-terminated silicon substrates for low-temperature molecular beam epitaxy," Thin Solid Films , vol. 183, pp. 197, 1989.

[10] T. L. Lin, J. S. Park, T. George, E. W. Jones, R. W. Fathauer, and J. Maserjian, "l. ong-wavelength PtSi infrared detectors fabricated by incorporating a p^+ doping spike grown by molecular beam epitaxy," Appl. Phys. Lett., vol. 62., pp. 3318-3320, 1993.

[11] J. I. Pankove, Optical Processes in Semiconductors, (Dover Publishers, New York, 1975), p. 67.

FIGURE CAPTIONS

Figure 1. The energy band diagram of the $Si_{1-x}Ge_x/Si$ HIP detector.

Figure 2. Reverse current-voltage characteristics of a typical 10-rim-thick $Si_{0.7}Ge_{0.3}/Si$ HIP detector with a 1.2 x 10^{-3} cm^2 detector area at various temperatures.

Figure 3. Plots of J_o/T^2 versus 1000/T for a typical 10-nm-thick $Si_{0.7}Ge_{0.3}/Si$ HIP detectors at a reverse bias of 0.5 V.

Figure 4. External quantum efficiency as a function of wavelength for the $Si_{0.7}Ge_{0.3}/Si$ HIP detector and the doping-spike PtSi detector.

Figure 5, Modified Fowler Plot of η hv versus hv for the $Si_{0.7}Ge_{0.3}/Si$ 1111' detector at a reverse bias of 0.5 V. C_h and Y'. were. determined from the slope and the intercept of the linear portion.

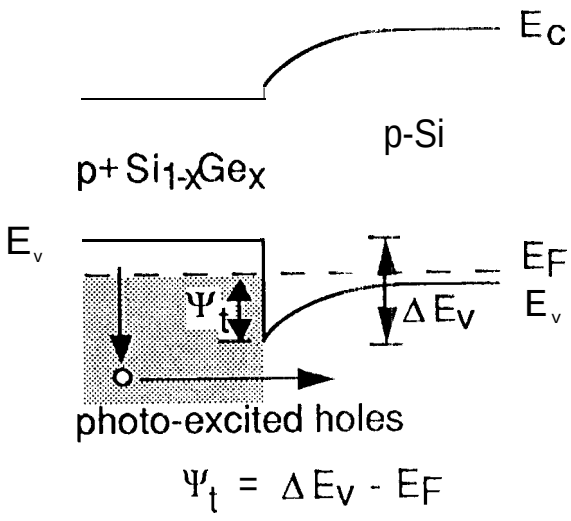

Figure 1. The energy band diagram of the $Si_{1-x}Ge_x$/Si HIP detector.

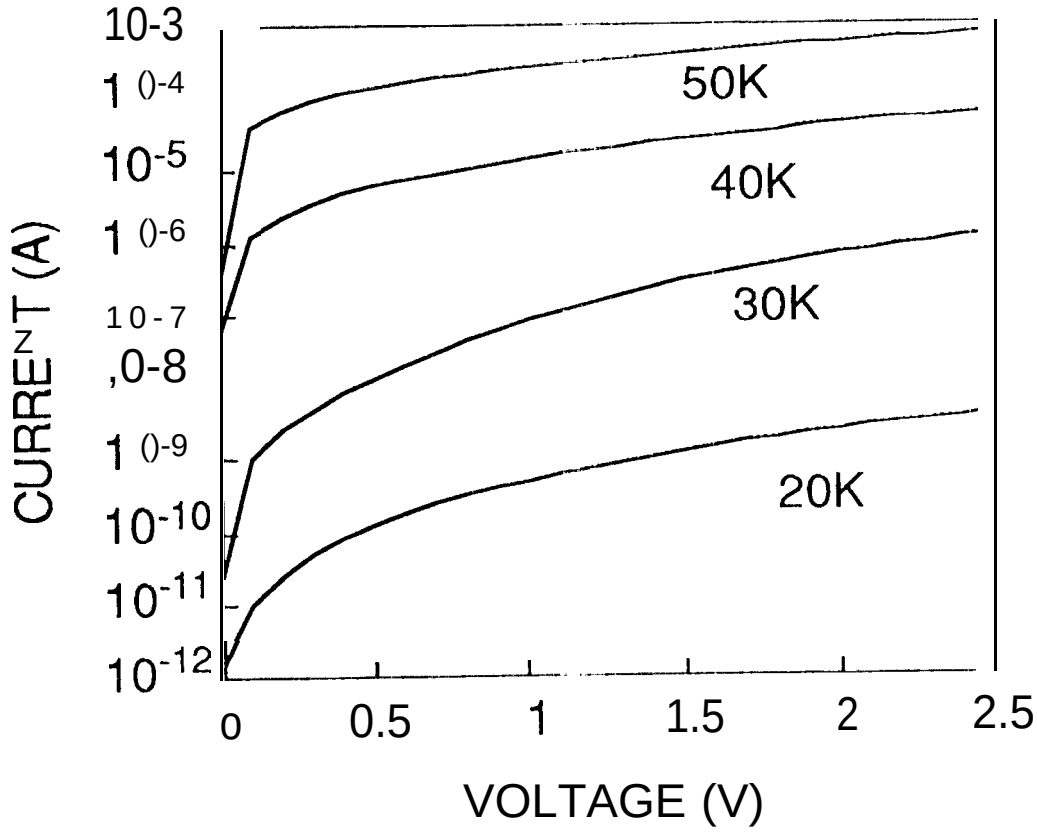

Figure 2. Reverse current-voltage characteristics of a typical 10-rim-thick $Si_{0.7}Ge_{0.3}$/Si HIP detector with a 1.2 x 10-3 cm^2 detector area at various temperatures.

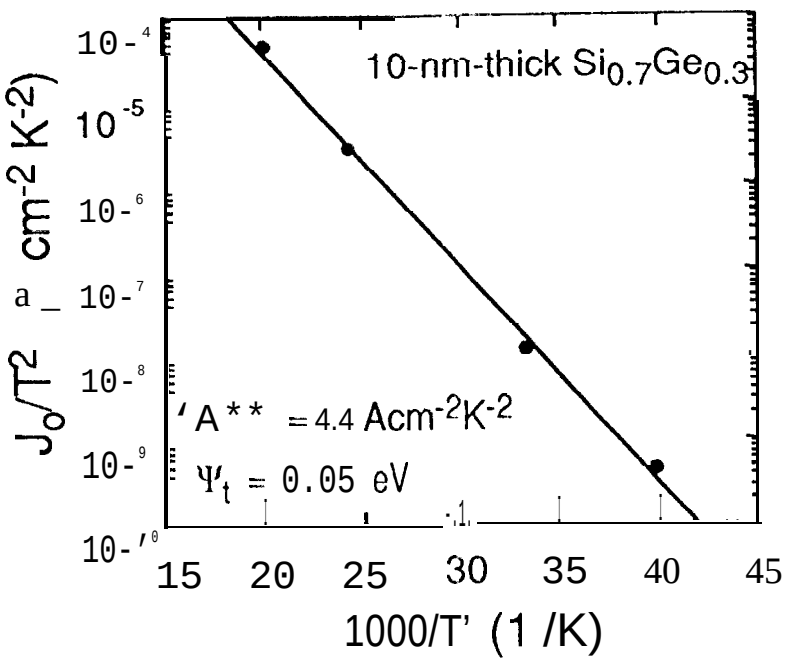

Figure 3. Plots of J_o/T^2 versus 1000/T for a typical 10-rim-thick $Si_{0.7}Ge_{0.3}$/Si HIP detectors at a reverse bias of 0.5 V.

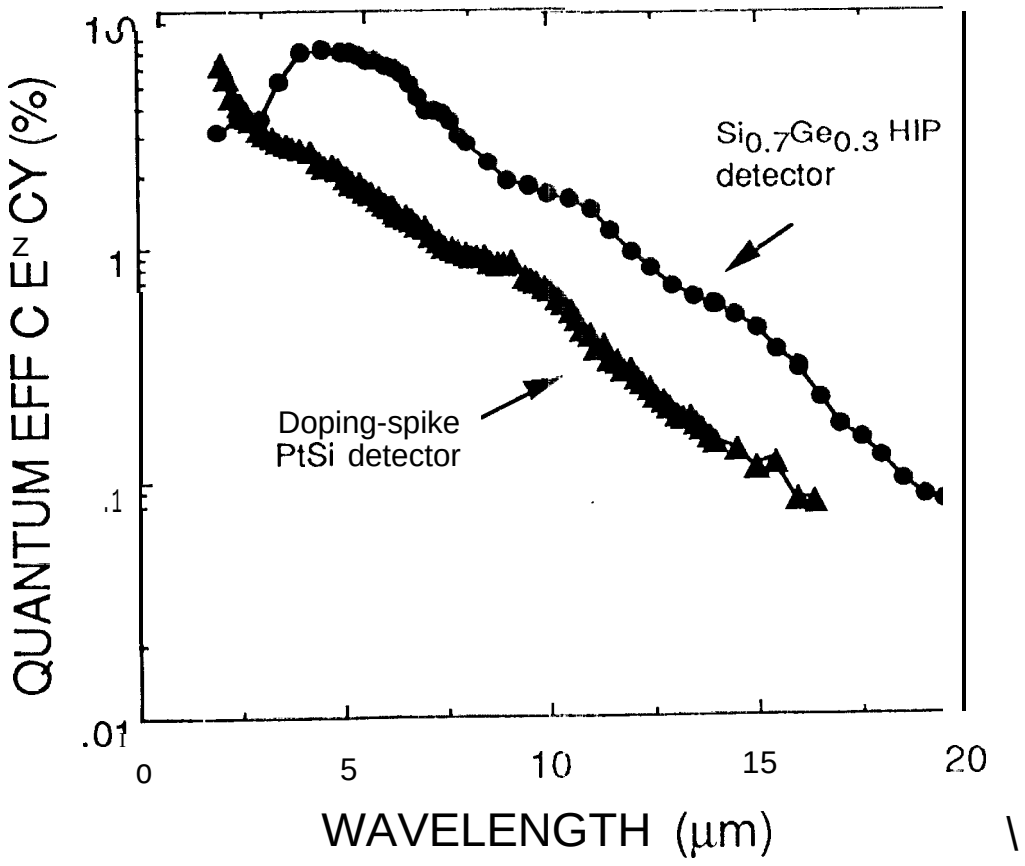

Figure 4. External quantum efficiency as a function of wavelength for the $Si_{0.7}Ge_{0.3}$/Si HIP detector and the doping-spike PtSi detector.

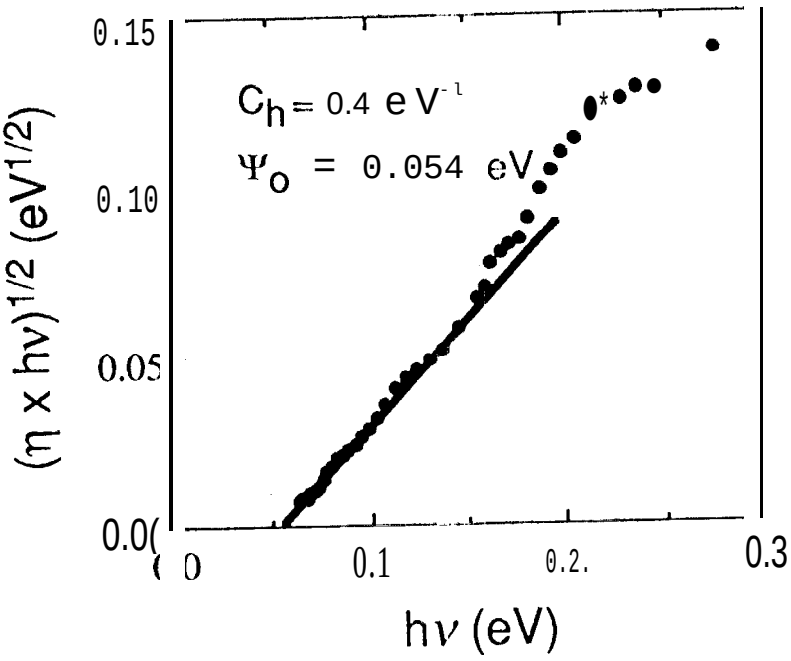

Figure 5. Modified Fowler Plot of $\sqrt{\eta\ h\nu}$ versus hv for the $Si_{0.7}Ge_{0.3}$/Si HIP detector at a reverse bias of 0.5 V. C_h and Ψ_o were determined from the slope and the intercept of the linear portion.